Arshad Ali[1], Nauman Ali Larik[2,*], Muhammad Faizan Tahir[2], Rabeh Abbassi[3], Houssem Jerbi[4], Kashif Mehmood[1]

J. Electrical Systems 16-3 (2020): 393-410

Regular paper

Modeling and Fault Characteristics Analysis of Doubly Fed Induction Generator Incorporating Crowbar Protection

The most widely used electrical energy plays the vital role in development and economy of any country as per capita use of energy straight linked with living standard. However, this energy is extensively produced by fossil fuels which are not only declining rapidly but also a threat to ecology system. Therefore, it encourages to project towards green society by incorporating more and more renewable energy in the system. Sustainability and cost-effectiveness of wind makes it most promising technology than the rest of renewable energy sources but uncertainty and variability makes it difficult to integrate in the system. Therefore, doubly fed induction generator (DFIG) which exhibits variable speed is required to address above issues. In this work, a stator flux oriented vector control technique is used to perform a decoupled control of active and reactive power. The DFIG power converter is protected by employing crowbar protection while short circuit which affects the fault characteristics. Thus, the symmetrical fault (ABC) and asymmetrical fault (BC) characteristics are analyzed while the protection system (Crowbar) is active and inactive. It was observed when asymmetric fault occurs on the collection line, the current of healthy phase is also increased at the turbine side and during symmetrical fault positive and negative sequence impedances of DFIG are not equal, unlike the traditional system.

Keywords: Doubly-Fed Induction Generator; Crowbar Protection; Fault Characteristics; Simulation Analysis
Article history: Received 18 July 2019, Accepted 3 July 2020

1. Introduction

The clean and sustainable energy has become essential need of modern society and plays a significant role for economic, social as well as human development. Since many decades fossil fuels, have driven our generating stations, supported industries and fuelled our vehicles but these are limited, expensive, depleting day by day [1, 2], and causes heavy risk for environment by the level of raising CO_2 [3]. Therefore, different international agencies promote use of green energy and encourage installing the renewable energy sources (RES) for producing electrical energy. Among available RES, wind is clean, sustainable and fastest developing source of energy recently installed capacity of wind in the world as reached up to 597 GW which shows 49 GW additions in only year 2018[20]. However, stochastic nature of wind imposes severe challenges for electric power utility to maintain continuity in supply and power quality [5]. Wind energy conversion systems (WECS) consists of wind turbine, to produce kinetic energy from wind source and doubly fed induction generator (DFIG) generator with controlling and protection system to generate electrical energy [6]. A special wound rotor induction generator named as DFIG in which not only stator but rotor is also connected with electrical source through power converter. It is preferred with wind turbine because it can be used with variable speed, cost effective and better efficiency [7].

Corresponding author: School of Electric Power, South China University of Technology, 510640 Guangzhou, China. E-mail: epnauman.ali@mail.scut.edu.cn
[1] Department of Electrical Engineering, Southeast University, 210096 Nanjing, China
[2] School of Electric Power, South China University of Technology, 510640 Guangzhou, China.
[3] Department of Electrical Engineering, College of Engineering, University of Ha'il, Hail, Saudi Arabia.
[4]Department of Industrial Engineering, College of Engineering, University of Ha'il, Hail, Saudi Arabia.

Copyright © JES 2020 on-line : journal.esrgroups.org/jes

Various papers attempt to describe the advantages of a variable-speed system (i.e. based on DFIG) from different aspects like In [8] it is stated that the 2-3% system efficiency can be improved with DFIG. In [9] a comparison of doubly fed induction machine with variable and fixed speed system is well presented, based on operating region and energy output, the DFIG-based energy production can be increased above 20% as compared to variable speed cage-bar induction generator and 60% with respect to the fixed speed system. These variations in results causes the assumptions applied, control strategy, design aspects and as it is declared in [10] that energy output depends on the method applied for MPPT.
In literature DFIG-based wind turbine is used to realize decoupled active and reactive power control. In [3], the evolution from fixed speed to variable speed increased their ability to extract optimum wind energy, besides that a power converter interfacing enables to control the active and reactive power [8, 11]. In [7], vector control method is employed for decoupled control of active and reactive power is presented control to keep that stator at unity power factor and attain maximum power. According to 12 faults ride through (FRT) enables the generator to work properly and connected with network from disconnecting during fault or any transient disturbance. In [13], crow bar protection is proposed for protecting power converter connecting the rotor windings and the grid need to protect during short circuits. According to [14], by controlling rotor current ensures efficient operation in sub synchronous and super synchronous modes. So for controlling rotor current, several vector control or direct torque schemes have been documented [10, 15]. Generally with stator-flux orientation [7, 8, 15, 16, 17], or with air-gap-flux orientation is used for controlling the rotor current.
The contribution of this research work is to analyse the influence of doubly fed induction generator on the traditional system fault characteristics. The doubly fed induction generator modelling is depicted in detail with equations by using PSCAD software and fault characteristics analysis is shown based on simulation results. Moreover, in this paper different fault conditions with different locations while the Crowbar is active or inactive and its respective effect on fault characteristic are also considered.
This paper is organized as follows: Section 2 provides doubly fed induction generator modelling where Power converters controlling methods with over current protection (crow bar) are simulated in PSCAD/EMTDC software. Section 3 presents theoretical analysis of impedance of both sides where one side is utility grid and other is DFIG. Later we analysed fault characteristics of DFIG based wind farm interconnected with grid under different faults with or without crowbar protection, based on simulation results the characteristics of each fault is summarized in analysis. Finally, section 4 concludes the paper.

2. System Modeling

DFIG based wind turbine model is used in this work which is shown in Fig.1.

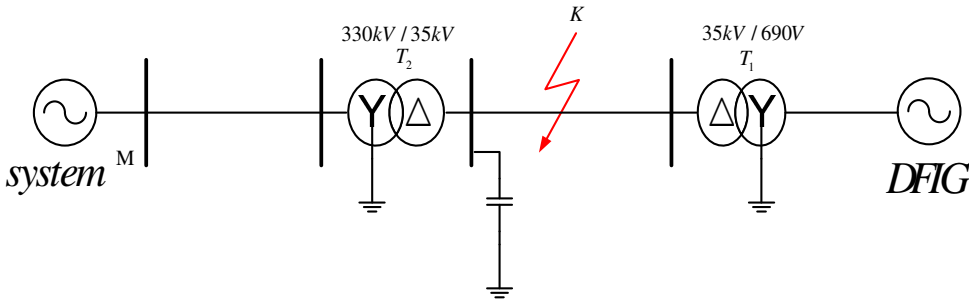

Fig.1 Single line diagram of the model

2.1 System Configuration

Wind turbine model	Wind turbine radius	38.68 m	Air density	1.225 g/m3
	DFIG rotor speed ω	1.167	wind speed	11m/s
DFIG model	Rated voltage	0.69 kV	Rated capacity	1.5 MVA
	Stator resistance	0.007 pu	Rotor resistance	0.008 pu

3.2 Modeling Description

Two back-to-back PWM voltage source converters, one at generator-side and other at grid-side has been used in given model with DC-link capacitor [8], which is equipped with IGBTs provided with freewheeling diodes to enable a bi-directional power flow.

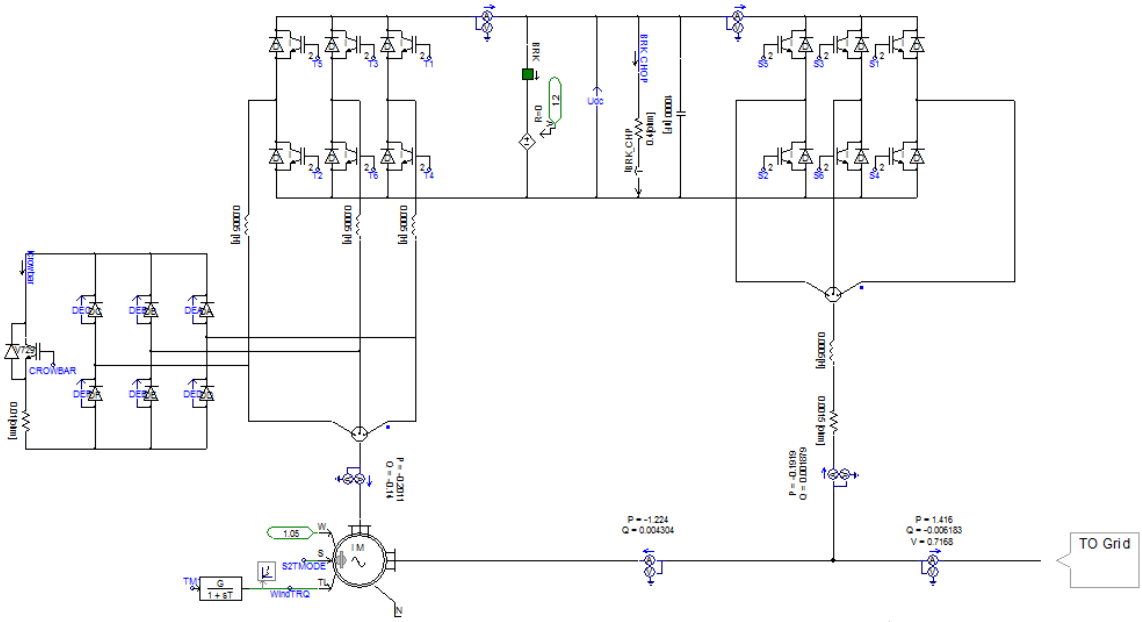

Fig.2 PSCAD model DFIG converter

The equivalent circuit by applying KVL in both stator and rotor loop and the direct-quadrature (d-q) model of DFIG is represented in [19] which illustrated in Fig.3.

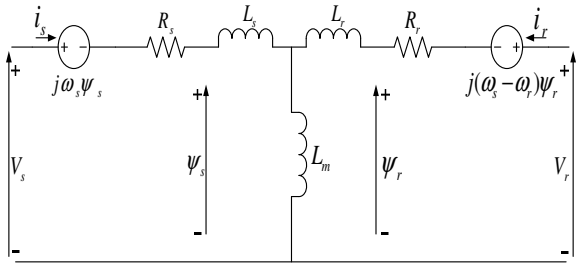

Fig.3 Equivalent circuit of DFIG

According to [19];

$$\begin{cases} v_{sd} = R_s i_{sd} + \dfrac{d\psi_{sd}}{dt} - \omega_s \psi_{sq} \\ v_{sq} = R_s i_{sq} + \dfrac{d\psi_{sq}}{dt} + \omega_s \psi_{sd} \end{cases} \quad (1)$$

$$\begin{cases} v_{rd} = R_r i_{rd} + \dfrac{d\psi_{rd}}{dt} - (\omega_s - \omega_r)\psi_{rq} \\ v_{rq} = R_r i_{rq} + \dfrac{d\psi_{rq}}{dt} + (\omega_s - \omega_r)\psi_{rd} \end{cases} \quad (2)$$

The stator flux is obtained by, in $\alpha\beta$-components in stationary reference frame:

$$\begin{cases} \psi_{\alpha s} = \int (v_{\alpha s} - R_s i_{\alpha s})dt \\ \psi_{\beta s} = \int (v_{\beta s} - R_s i_{\beta s})dt \end{cases} \quad (3)$$

From equation (4), the stator flux angle is calculated as:

$$\phi_s = \tan^{-1}\left(\frac{\psi_{\beta s}}{\psi_{\alpha s}}\right) \quad (4)$$

Where, R_s, R_r, L_{ss}, L_{rr} showing the resistance and inductance of stator and rotor respectively and L_m is the mutual inductance, currents and flux represented as d-q components respectively (i.e. v_{sd}, v_{sq}, v_{rd}, v_{rq}, i_{sd}, i_{sq}, i_{rd}, i_{rq}, ψ_{sd}, ψ_{sq}, ψ_{rd} and ψ_{rq}), while ω_r is rotor speed in electrical degree. Both variable of stator and rotor are referred to the stator reference frame. Therefore, q-component of stator flux is null, whereas, d-component of stator flux equals to total flux. Thus decoupled control over the active and reactive power of the stator is obtained.

Let, stator winding resistance is neglected (i.e. R_s=0), then the stator voltage and flux can be simplified as

$$\begin{cases} \psi_{sd} = \psi_s = L_{ss} i_{sd} + L_m i_{rd} \\ \psi_{sq} = 0, \end{cases} \quad (5)$$

$$\begin{cases} v_{sd} = 0 \\ v_{sq} = V_s = \omega_s \psi_s \end{cases} \quad (6)$$

3.3. Power Converter Control

The vector control system employed in converter can be used to accomplish decoupled active and reactive power control and independent torque control as well as rotor excitation current. In a vector control system, a complex reference frame, $\alpha\beta$-frame is introduced to describe three phase voltage and current as a vector [13], which can make transformations easy a-b-c to d-q and d-q to a-b-c. The rotor current in d-q frame is controlled by providing an appropriate reference currents frame, which were injected by the voltage source converter. In order to get rotating reference frame, it is essential to get the instantaneous position of the rotating flux vector. The equation (3) determines the instantaneous position of rotating flux vector, which is the derivative of stator flux linkage per phase and can be achieved by subtracting the rotor resistive drop of the rotor.

$$\frac{d\psi_a}{dt} = v_a - R_a i_a \quad (7)$$

Such a control structure is modeled in PSCAD and illustrated in Fig. 4 which determines the location of rotating flux vector (ϕ_s).

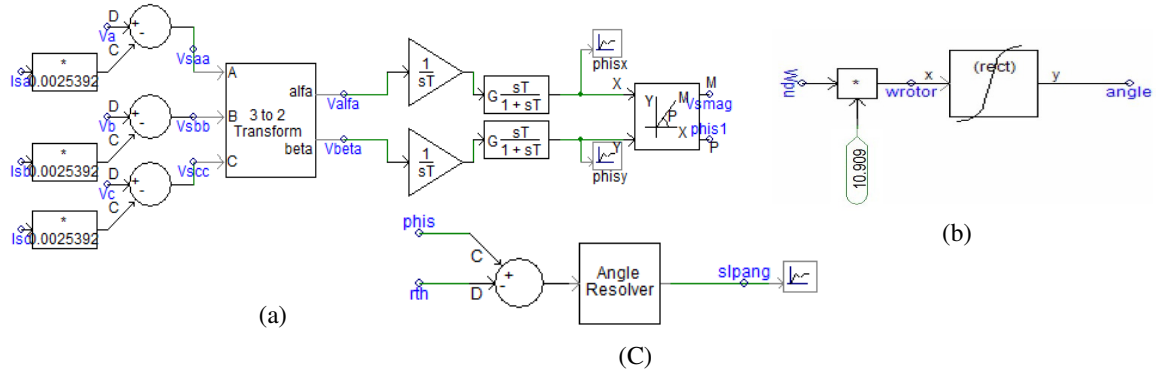

Fig.4 Control diagram for locating instantaneous position of rotating flux vector

Fig.4 (a) locates the current position of stator flux. Fig. 4(b) integrates the rotor speed to achieve rotor position and Fig. 4(c) interoperates the difference of stator flux and rotor position to fix on the current. Three- phase voltages have been converted in stationary reference frame as v_α and v_β after removal of stator voltage drop, under the steady state they are orthogonal. This transformation is given by:

$$\begin{bmatrix} v_\alpha \\ v_\beta \end{bmatrix} = \frac{2}{3}\begin{bmatrix} 1 & -\frac{1}{2} & \frac{1}{2} \\ 0 & \frac{\sqrt{3}}{2} & -\frac{\sqrt{3}}{2} \end{bmatrix}\begin{bmatrix} v_a \\ v_b \\ v_c \end{bmatrix} \tag{8}$$

The stator flux ψ_α and ψ_β can be calculated by integrating v_α and v_β components, and is given in polar from

$$|\psi| = \sqrt{\psi_\alpha^2 + \psi_\beta^2}, \phi_s = \tan^{-1}\left(\frac{\psi_\beta}{\psi_\alpha}\right) \tag{9}$$

The major task of the grid side converter is to keep constant DC-link voltage. A vector control technique is implemented with a reference frame oriented along with the stator voltage vector position, by which the decoupled control of active and reactive power can be enabled. Whereas, the converter is current regulated, therefore, both d and q current components have an individual out response like DC bus voltage can vary by i_d and i_q can regulate the reactive power. A schematic diagram of the grid side converter is illustrated in Fig.5.

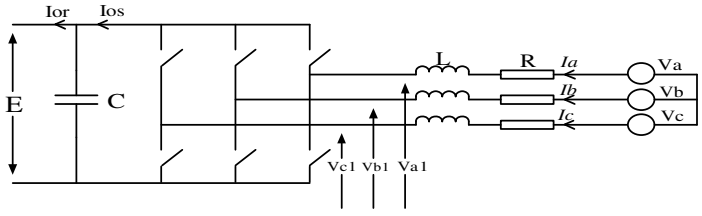

Fig.5 A Grid side converter illustration

The balance voltage represented as below,

$$\begin{bmatrix} v_a \\ v_b \\ v_c \end{bmatrix} = R\begin{bmatrix} i_a \\ i_b \\ i_c \end{bmatrix} + L\frac{d}{dt}\begin{bmatrix} i_a \\ i_b \\ i_c \end{bmatrix} + \begin{bmatrix} v_{a1} \\ v_{b1} \\ v_{c1} \end{bmatrix} \tag{10}$$

Where, v_a, v_b, and v_c are three phase supply voltages, i_a, i_b and i_c are three phase supply currents, v_{a1}, v_{b1}, and v_{c1} are the stator terminal voltages, R and L are the resistance and inductance respectively of supply line. The equation (10) in d-q reference frame can be represented with ω_e.

$$v_d = Ri_d + L\frac{d}{dt} - \omega_s L i_q + v_{d1}$$

$$v_q = Ri_q + L\frac{d}{dt} + \omega_s L i_d + v_{q1}$$

By definition v_q is zero and v_d remain constant as the magnitude of grid voltage constant. Therefore, active and reactive power will be controlled individually by i_d and i_q respectively.

$$\begin{cases} P = \frac{3}{2} v_d i_d \\ Q = -\frac{3}{2} v_d i_q \end{cases} \tag{11}$$

If the switching harmonics, inductive resistance and converter losses are neglected, thus we have,

$$Ei_{os} = 3v_d i_d \tag{12}$$

$$v_d = \frac{m_1}{2\sqrt{2}} E \tag{13}$$

$$i_{os} = \frac{3}{2\sqrt{2}} i_d m_1 \tag{14}$$

$$C\frac{dE}{dt} = i_{os} - i_{or} \tag{15}$$

Hence from equation (13) and (14), the DC-link voltage can be controlled by i_d. Moreover, current controls loops are used for i_d and i_q, where desired id derived from standard PI controller, by using DC-link voltage error.

3. Fault Characteristic Analysis

3.1 Impedance Analysis

Fig.6 is illustrates the power system integrated with doubly fed induction generator, whereas the Fig7 demonstrates the fault network of the given system. When a line to line fault occurs in between the two buses m and n.

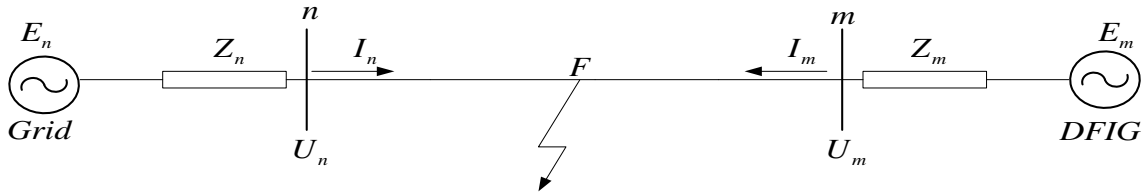

Fig. 6 System diagram integrated with DFIG

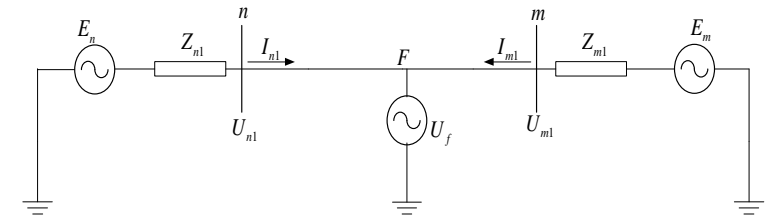

(a) Positive sequence network

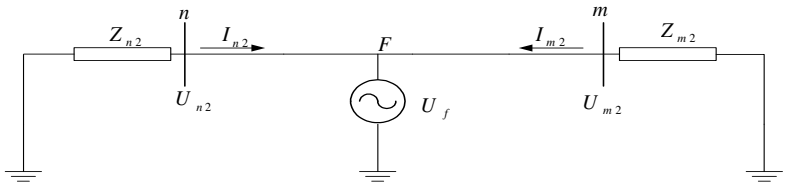

(b) Negative sequence network

Fig.7 Fault network of the system integrated with DFIG

The system impedance of grid side and DFIG can be defined as in symmetrical components. From Fig.8 (a) the positive and negative sequence impedancee of grid side is as follows, Ohm's law:

$$\begin{cases} Z_{1n} = -\dfrac{\triangle U_{1n}}{\triangle I_{1n}} \\ Z_{2n} = -\dfrac{\triangle U_{2n}}{\triangle I_{2n}} \end{cases} \tag{16}$$

According to line to line fault characteristics of voltage and current $Z_{1n} = Z_{2n}$ Suppose $E_{1m(0)}$ and $E_{1m(t)}$ is the pre-fault and during fault voltage respectively, generated by DFIG. Similarly, $U_{1m(0)}$, U_{1m} and $I_{1m(0)}$, I_{m1} are the bus voltages and currents before and during fault respectively. According to Ohm's law the DFIG side positive sequence impedance can be calculated from Fig. 8(a) as follows:

$$\begin{cases} U_{1m(0)} = E_{1m(0)} - Z_{1m} I_{1m(0)} \\ U_{1m} = E_{1m(t)} - Z_{1m} I_{1m} \end{cases} \tag{17}$$

Thus, the calculated positive sequence impedance (Z_{1cal}) can be written as:

$$Z_{1cal} = -\frac{\triangle U_1}{\triangle I_1} \tag{18}$$

$$Z_{1cal} = -\frac{\left(E_{1m(t)} - Z_{1m} I_{1m} - E_{1m(0)} + I_{1m(0)}\right)}{\triangle I_{1m}} \tag{19}$$

$$Z_{1cal} = Z_{1m} - \frac{\left(E_{1m(t)} - E_{1m(0)}\right)}{\triangle I_1} \tag{20}$$

From the eq.20 can be seen, that the protection can identify Z_{1m} plus an additional impedance because of change in generated voltage $E_{1m(t)}$ and $\triangle I_{1m}$. During the fault, the wind control system cannot get itself to the stable state. It remains in the state of adjusting, so the $E_{1m(t)}$ keep changing until the fault steady state and it is the exact reason for the instability of the positive sequence impedance of the wind turbine.

3.2 Fault Analysis

We analyze the influence and a fault characteristic of DFIG connected with grid, So far, all faults occur on the middle of 35kV medium voltage transmission line, it is to analyze the system behavior under three-phase ABC and two-phase BC fault because the system is grounded indirectly. The observation is made in both cases while the crowbar is active or inactive, while the data is taken at three points, turbine side, grid side and generator output terminals. Where the fault initiating time is 3.2sec and the determined fault duration is 0.2 sec.

3.2.1 Three Phase fault Without Crowbar Protection

Three-phase fault is a balanced fault, in which all three phases brought into short circuit simultaneously. It is very rare occurring but most severe in all types of fault. Here, we analyze a three-phase fault without applying crowbar protection. As it is balanced fault, therefore, neither negative nor zero-sequence currents are present. Thus only the positive-sequence network is used.

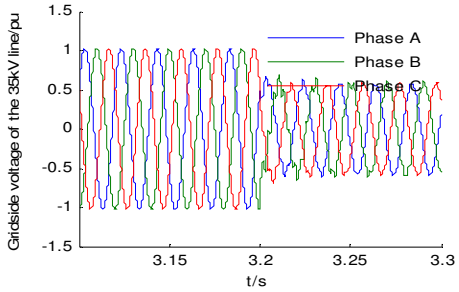

(a) Grid side three phase voltage

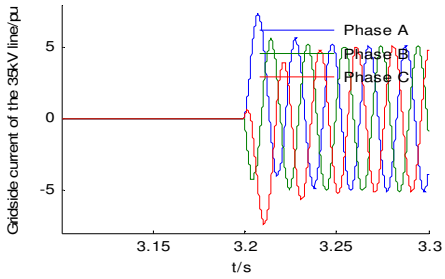

(b) Grid side three phase Current

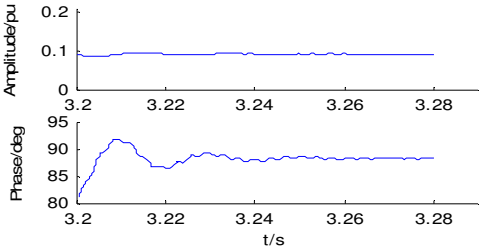

Positive sequence impedance

Fig.8 Grid side wave Forms under ABC fault

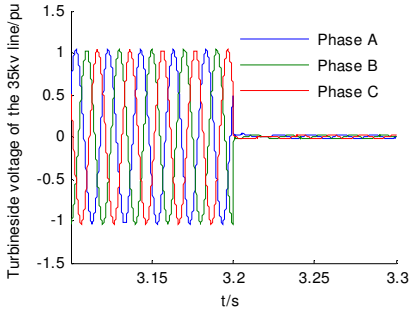

(a)Turbine side three phase voltage

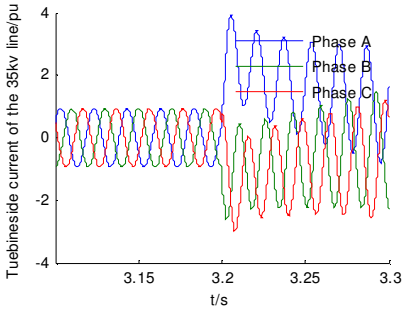

(b) Turbine Side three phase current

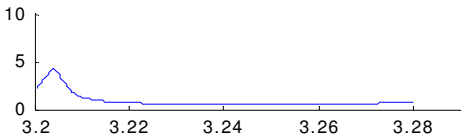

(c)Positive sequence impedance

Fig.9 Turbine side wave Forms under ABC fault

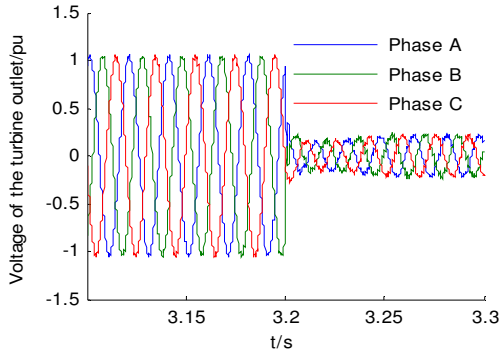

(a) Turbine Terminal three phase voltage

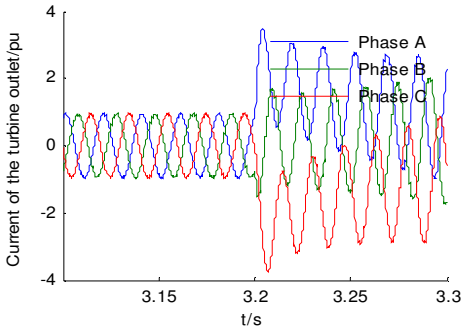

(b) Turbine terminal three phase current

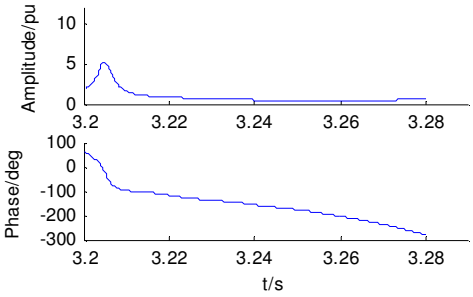

(c) Positive sequence impedance

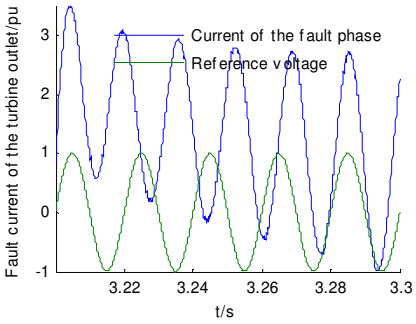

(d) Fault phase Current

Fig. 10 Turbine terminal wave Forms under ABC fault

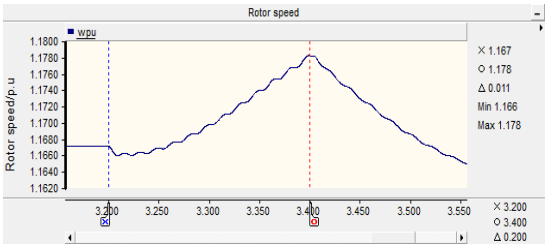

Fig. 11 Rotor speed

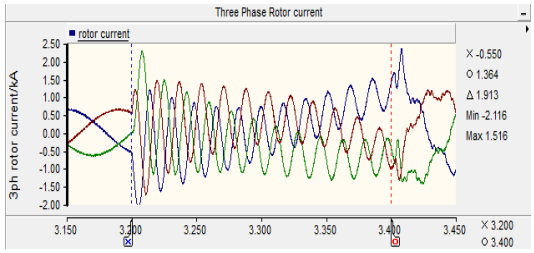

Fig. 12 Rotor current

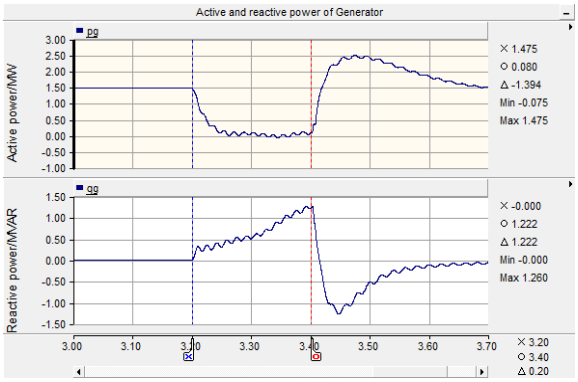

Fig.13 Active and reactive power of generator

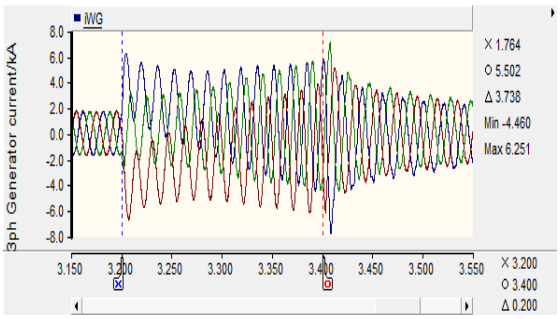

Fig.14 Three phase generator current

Analysis

From Fig. 8(a), 9(a) and 10(a), it has been observed that when fault occurs, there is a voltage drop at all, but the voltage of the turbine side fall nearly to zero as compared to grid side voltage, while the turbine terminal voltage ¼ times of its nominal voltage after fault. The Fig. 8(b), 9(b) and 10(b) determine the characteristics of three-phase current, where it

has been noticed that all currents increased but the grid side three phase currents contribute more and decay slower than the turbine side. Though it is three phase fault therefore only positive sequence network is used. Fig.8(c), 9(c) and 10(c) represent positive sequence impedance. From the figures, it has been seen that grid side impedance remain stable even after fault, while turbine side impedance increased initially for 2-3ms after fault then decay gradually and stabilized. Its phase angle decreases continuously. The fault characteristic of the impedance of turbine terminal is similar to turbine side on 35kV line. Further, when the fault occurs there the rotor speed is increased from 1.167p.u to about 1.178p.u, the rotor three phases current is increased about 1.5 times the rated value of rotor as shown in Fig. 11 and Fig. 12 respectively. After the fault clearance, the voltage attains their nominal values and the rotor current also reduced. As shown in Fig.13 the active and reactive powers suddenly changed, the active is decreased to zero and the reactive increased and vice versa after fault. Finally, the Fig.14 depicts the sudden rise about three times the nominal value in generator current.

3.2.2 Phase to phase fault without Crowbar Protection

Phase to phase fault is an asymmetrical type and here it is applied by considering phase B and C, on the middle of 35kV medium voltage line and observed from different points of the system while the crowbar is inactive.

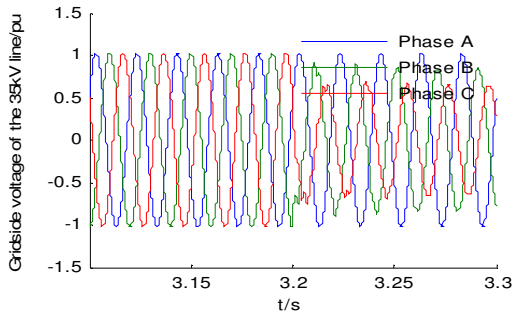

(a) Grid side three phase voltage

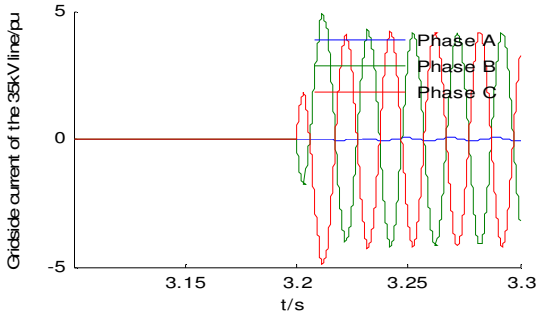

(b) Grid side three phase Current

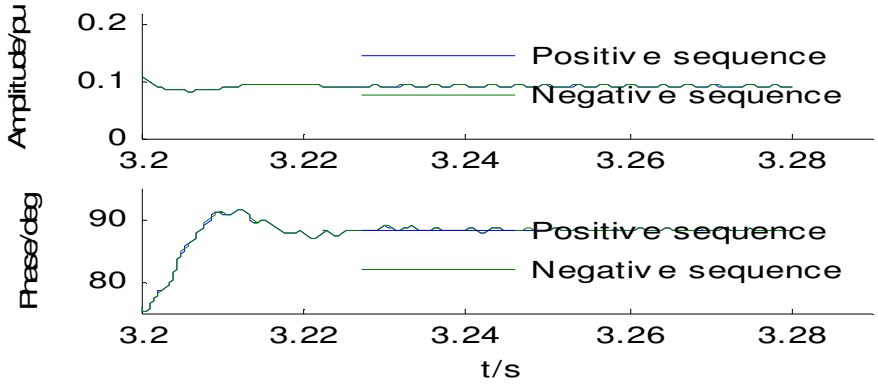

(c)Positive-negative sequence impedance

Fig. 15 Grid side wave Forms under BC fault

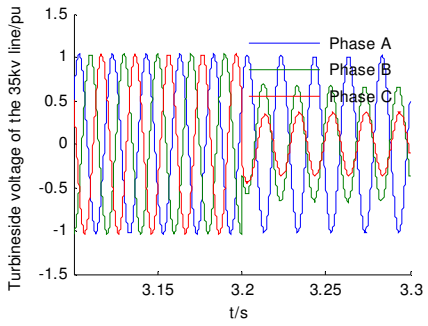

(a)Turbine side three phase voltage

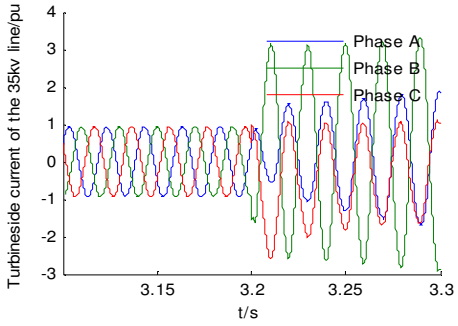

(b) Turbine Side three phase current

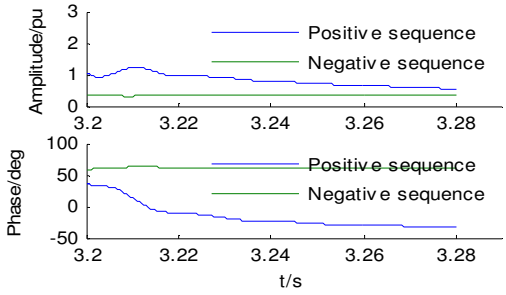

(c)Positive-negative sequence impedance

Fig. 16 Turbine side wave Forms under BC fault

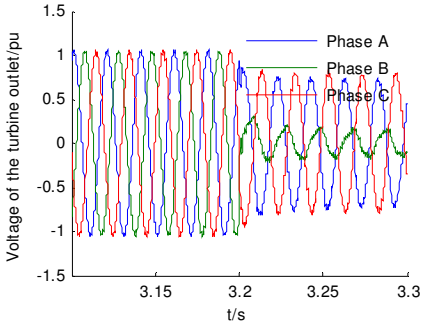

(a)Turbine Terminal three phase voltage

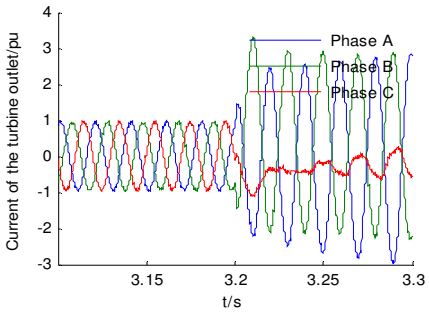

(b) Turbine terminal three phase current

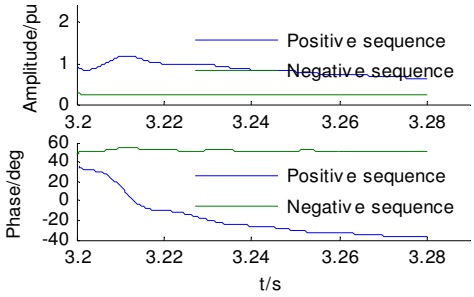

(c) Positive-negative sequence impedance

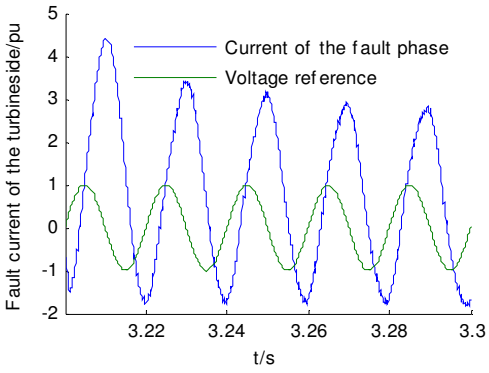

(d) Fault phase current

Fig. 17 Turbine terminal wave Forms under BC fault

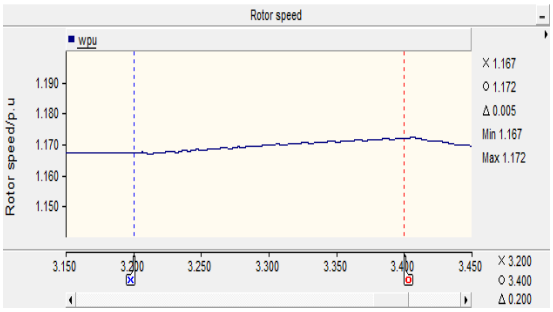

Fig. 18 Rotor speed

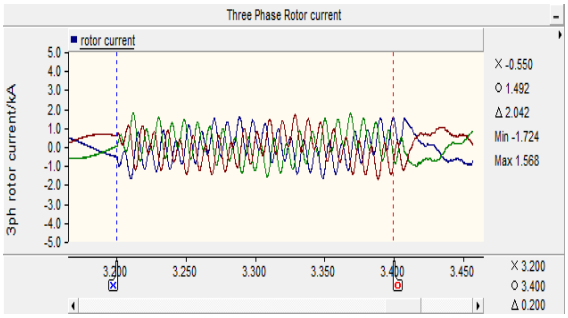

Fig. 19 Rotor current

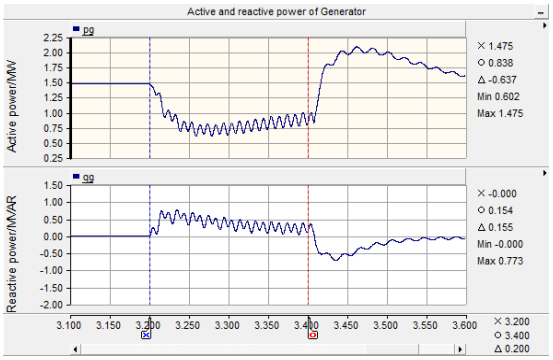

Fig. 20 Active and reactive power of generator

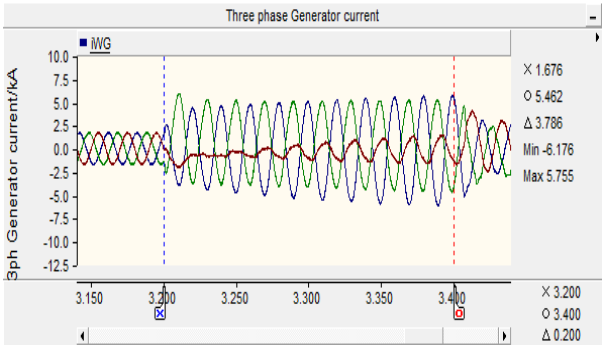

Fig. 21 Three phase generator current

Analysis

From Fig. 15(a), 16(a) and 17(a) it has been observed that when the fault occurs, the grid side voltage of A-phase remains stable, while the voltage of phase B and C slightly fall down almost with same phase angle with respect to their nominal voltage before fault. Similar behavior of voltage of phase B and C on the turbine side is noticed in addition the A-phase voltage is also decayed slightly. In Fig. 15(b), 16(b) and 17(b) it has been noticed that the grid side current of phase B and C increased with opposite phase angle and of A-phase remains stable. While the three- phase currents of the turbine side and turbine terminal are increased initially then decay. Unlike the three to ground fault, here negative sequence impedance is included. Fig. 15(c), 16(c) and 17(c) it has been seen that the grid side positive-negative sequence remains stable and equal even after a fault. Also, the negative sequence impedance of the turbine side doesn't change, while positive sequence impedance initially increases then decreases and finally stabilized, further, remains slightly greater than negative sequence impedance. Similarly, at turbine terminal, negative sequence impedance does not change and positive sequence impedance increased initially and remains greater than negative sequence impedance. When the fault occurs, it seems that turbine terminal current frequency is increased but about negligible, shown in Fig.17 (d) and the rotor three phases current is increased about double of the rated value as shown in Fig.18 and Fig.19 respectively. After the fault clearance, the voltage attains their nominal values and rotor current also reduced.

3.2.3 Three phase fault With Crowbar Protection

Here we investigate three phase fault from different location with crowbar protection.

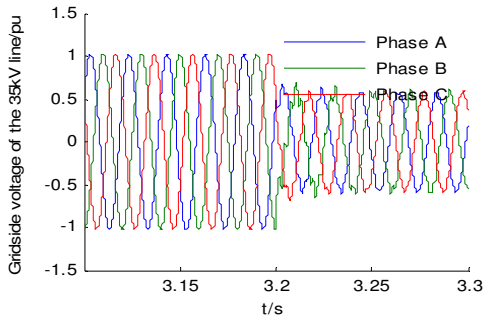

(a)Grid side three phase voltage

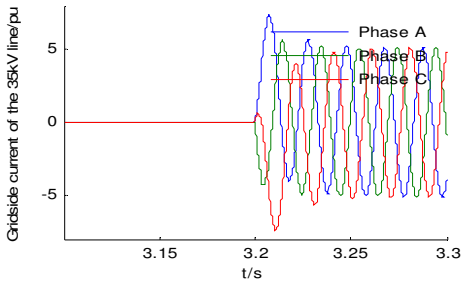

(b) Grid side three phase Current

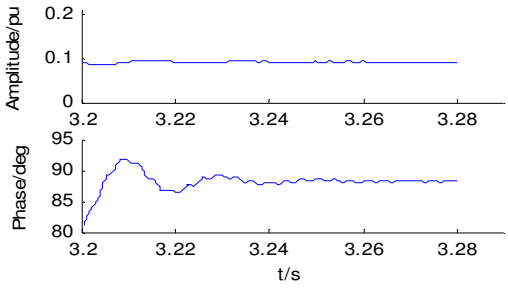

(c) Positive sequence impedance

Fig. 22 Grid side wave Forms under ABC fault

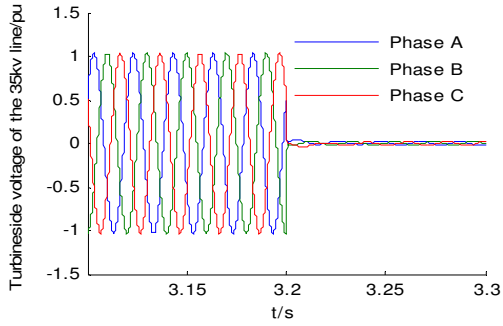

(a)Turbine side three phase voltage

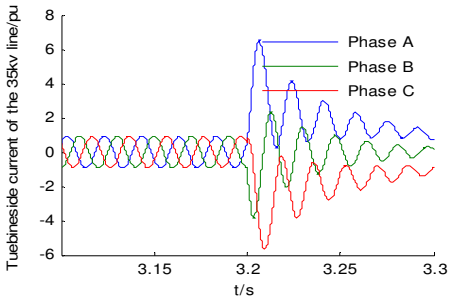

(b) Turbine Side three phase current

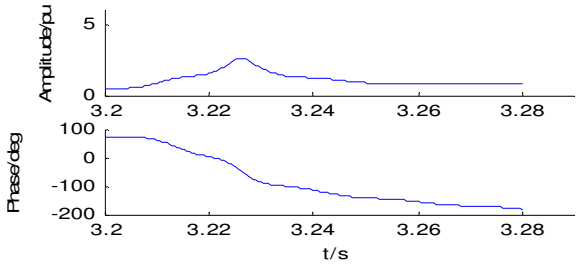

(c)Positive sequence impedance

Fig. 23 Turbine side wave Forms under ABC fault

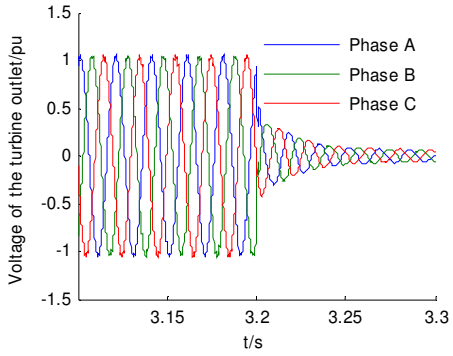

(a)Turbine Terminal three phase voltage

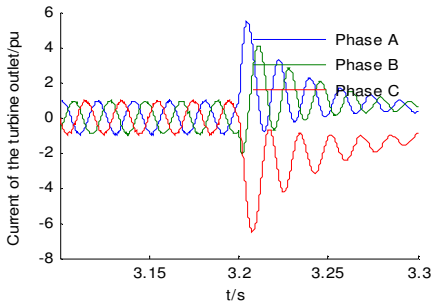

(b) Turbine terminal three phase current

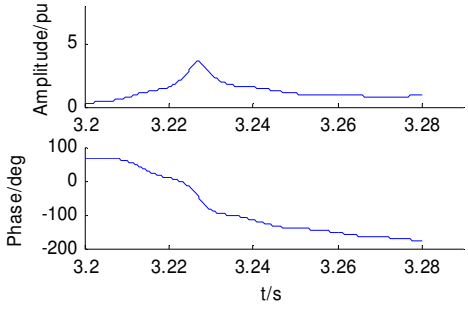

(c)Positive sequence impedance

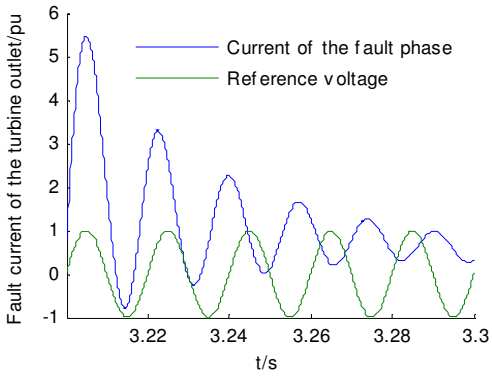

(d) Fault phase current

Fig. 24 Turbine terminal wave Forms under ABC fault

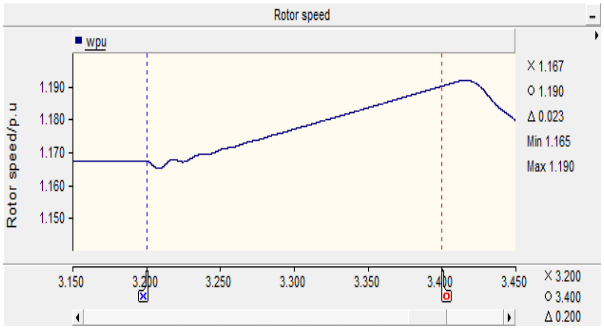

Fig. 25 Rotor speed

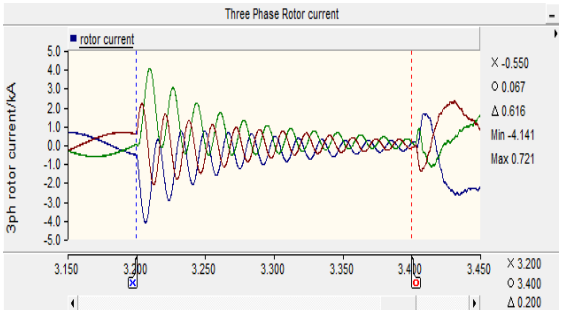

Fig. 26 Rotor current

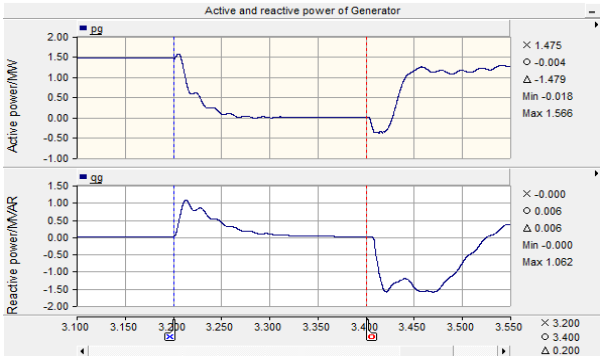

Fig. 27 Active and reactive power generator

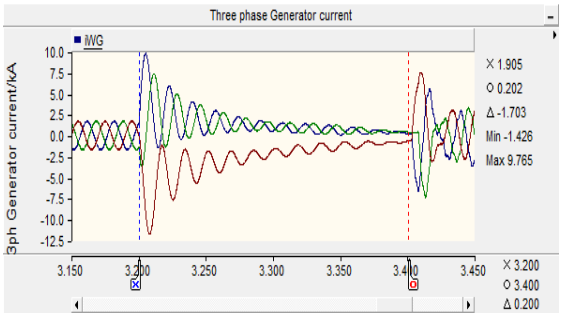

Fig. 28 Three phase generator current

Analysis

From Fig. 22(a), 23(a) and 24(a), we observe when a fault occurs, there is same voltage dip at grid side and turbine side even with crowbar as in previous case when it was inactive, while the turbine terminal voltage decreased afterwards gradually unlike the previous case. The Fig. 22(b), 23(b) and 24(b) find out the characteristics of three- phase current, where it

has been noticed that all currents increased, but the grid side three phase currents remain unchanged even after crowbar. While the turbine side and turbine terminal currents decreased quickly to safe operation in case of a crowbar. The positive sequence impedance is shown in Fig. 22(c), 23(c) and 24(c) as compared to the previous case, the grid side remains stable like the previous case, while the turbine side and turbine terminal impedance with the crowbar the impedance increased and decreased but at a slower rate. Further, from the Fig.25 and Fig.26 when the fault occurs the rotor speed is increased from 1.167p.u to about 1.19p.u, the rotor three phases current is increased but with a crowbar the current is decreased as compared to the previous case, this ensures the safe operation of rotor. Thus the DFIG is run as an ordinary induction machine, instead of getting the machine to trip. Hence the machine can ride through the fault. From the Fig.27 and Fig.28, we can say that there is a support of reactive power from DFIG for the support of voltage stability. Moreover, after the fault, when crowbar is no longer active, the DFIG draws a huge power till the rotor converter comes back in operation, the active power remains in support to the grid before reaching zero. While the three-phase generator currents are also reduced rapidly to safe values.

3.2.4 Phase to phase fault with Crowbar Protection

In this part we investigate phase to phase fault by considering crowbar protection.

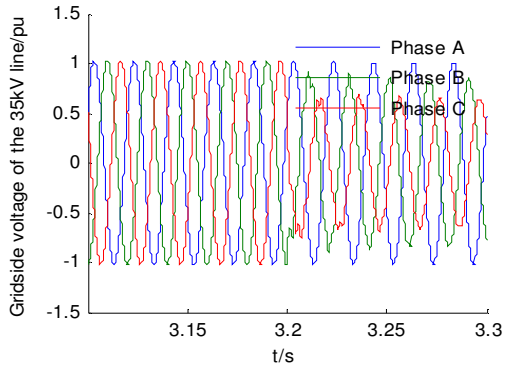

(a) Grid side three phase voltage

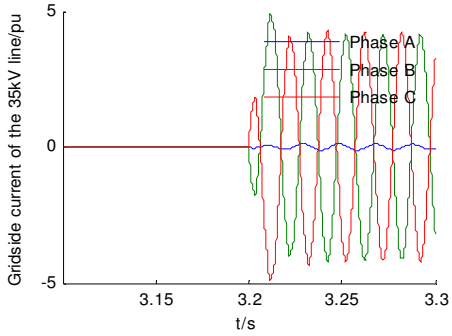

(b) Grid side three phase Current

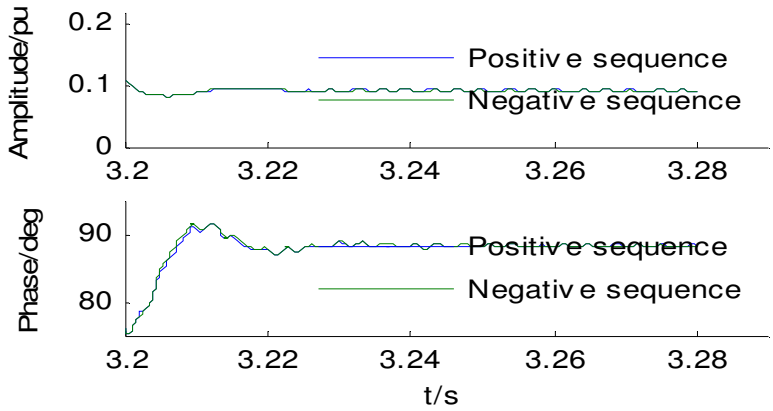

(c)Positive-negative sequence impedance

Fig. 29 Grid side wave Forms under BC fault

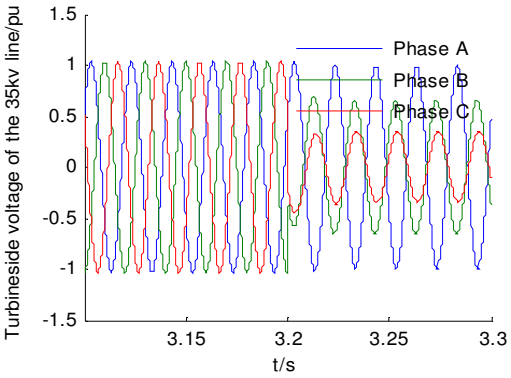

(a)Turbine side three phase voltage

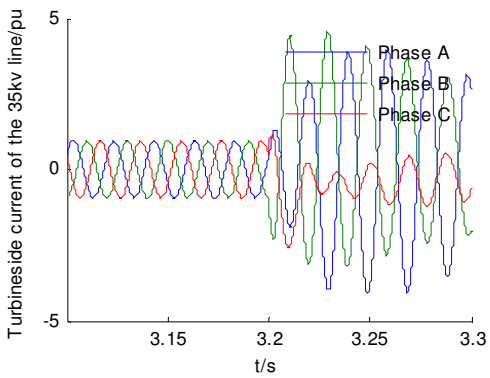

(b) Turbine Side three phase current

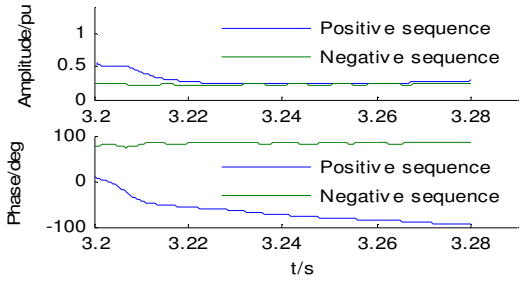

(c)Positive-negative sequence impedance

Fig.30 Turbine side wave Forms under BC Fault

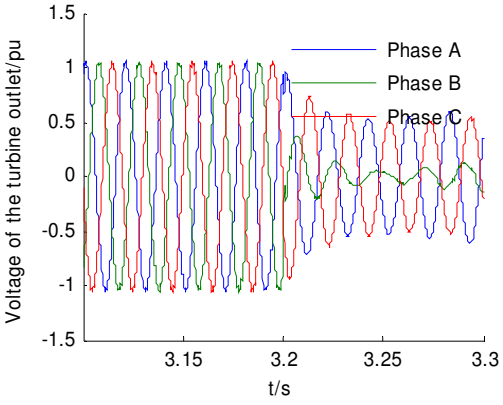

(a)Turbine Terminal three phase voltage

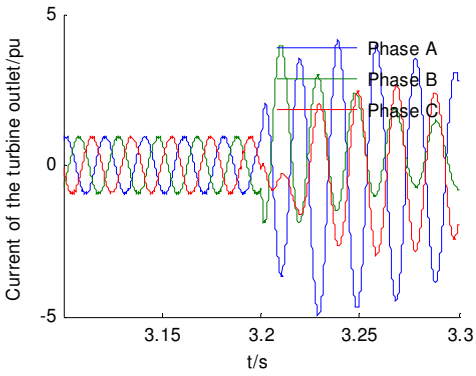

(b) Turbine terminal three phase current

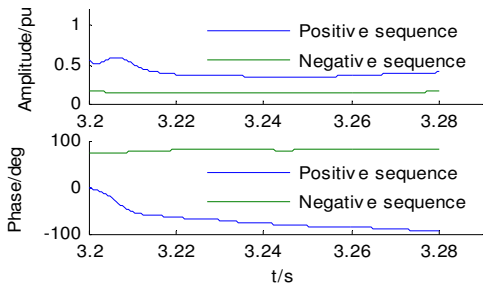

(c)Positive-negative sequence impedance

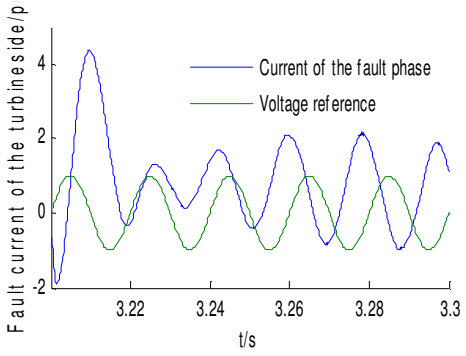

(d) Fault phase current

Fig.31 Turbine terminal wave Forms under BC fault

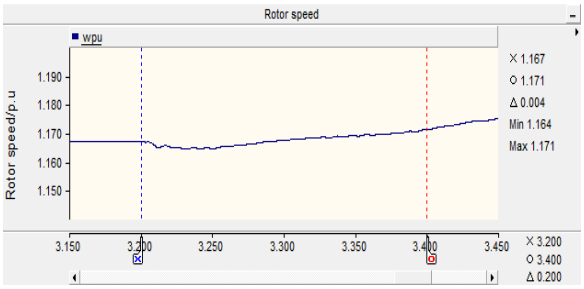

Fig. 32 Rotor speed

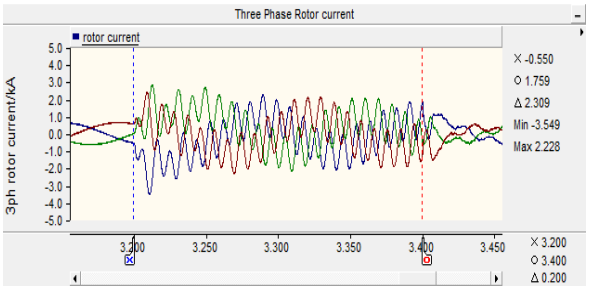

Fig.33 Rotor current

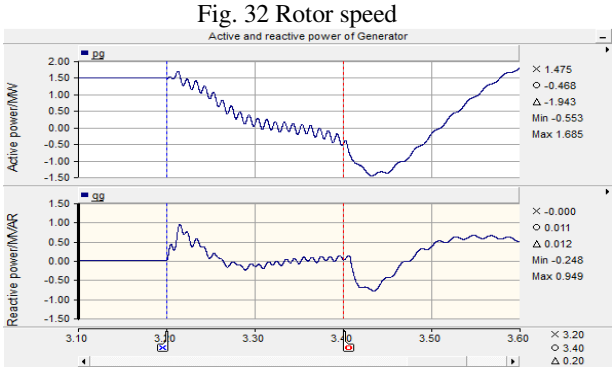

Fig. 34 Active and reactive power of generator

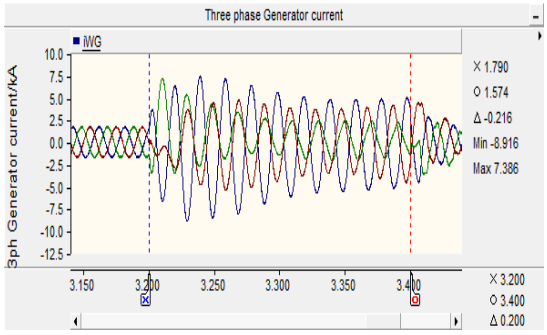

Fig.35 Three phase current of generator

Analysis

From Fig. 29(a), 30(a) and 31(a), like the previous case when the fault occurs, the grid side voltage of A-phase remains stable, while the voltage of phase B and C slightly fall down almost with same phase angle with respect to their nominal voltage. Similar behaviour of voltage of phase B and C on turbine side is noticed in addition the A-phase voltage has also decayed slightly. Finally, at the turbine terminal, the voltages decreased randomly, which is obviously a non-traditional system characteristic. It can be observed from Fig. 29(b), 30(b) and 31(b) that three phase currents of turbine side and turbines terminal are slightly reduced with a crowbar. The Fig. 29(c), 30(c) and 31(c) represent that the grid side positive-negative sequence remains stable and equal even after a fault in both cases. While turbine side positive sequence impedance initially increases then decreases and finally stabilized almost become equal to negative sequence impedance. Similarly, at the turbine terminal, negative sequence impedance does not change and positive sequence impedance increased initially and remains greater than negative sequence impedance like in case when crowbar was inactive.Further, when the fault occurs the rotor speed is increased, shown in the Fig.32 and fig.33, reduction in speed as compared to the previous case, the rotor three phases current is increased but reduces rapidly, this ensures the safe operation of the rotor. Moreover, after the fault, when crowbar is no longer active, the DFIG draws a huge power till the rotor converter comes back in operation, the active power remains in support to the grid before reaching zero. While the three-phase generator currents are also reduced rapidly to safe values.

Conclusion

The detailed modeling of DFIG for controlling the DFIG rotor current has been carried out in this paper. A stator flux oriented vector control method is adopted in d-q reference frame and it has been observed that the electromagnetic torque and stator active power control can be achieved by controlling the rotor current component. The theoretical analysis of impedance of DFIG and grid side has been carried-out that determines the positive and negative sequence impedance is equal in case of grid, but this is not true in case of DFIG because there is an additional impedance in positive sequence due to presence source and it's variation during fault in positive sequence network, thus the positive sequence

impedance fluctuates and negative sequence impedance remain stable which is analyzed from the simulation results. The analysis is based on the simulation results where DFIG is used under both conditions with or without crowbar and, two faults are chosen for the analysis one from symmetrical faults (ABC) and one from unsymmetrical faults (BC), moreover, the point to apply the fault is chosen 35kV line also called collecting line. It was found that when the crowbar is in active, the starting value and transient value of positive sequence impedance of collection line of the turbine side is greater than the grid side and the positive sequence impedance is greater than the negative sequence impedance due to presence of source in positive sequence network.

References

[1] Jalali, Mansour. DFIG based wind turbine contribution to system frequency control. MS thesis. University of Waterloo, 2011.

[2] Mazari, Shukul. Control design and analysis of doubly-fed induction generator in wind power application. Diss. University of Alabama Libraries, 2009.

[3] Galdi, V., A. Piccolo, and P. Siano. "Exploiting maximum energy from variable speed wind power generation systems by using an adaptive Takagi–Sugeno–Kang fuzzy model." Energy Conversion and Management 50.2 (2009): 413-421.

[4] Couto, Antônio, et al. "Wind power participation in electricity markets—The role of wind power forecasts." 2016 IEEE 16th International Conference on Environment and Electrical Engineering (EEEIC). IEEE, 2016.

[5] Dowell, Jethro, and Pierre Pinson. "Very-short-term probabilistic wind power forecasts by sparse vector autoregression." IEEE Transactions on Smart Grid 7.2 (2015): 763-770.

[6] Yaramasu, Venkata, Bin Wu, and Jin Chen. "Model-predictive control of grid-tied four-level diode-clamped inverters for high-power wind energy conversion systems." IEEE transactions on power electronics 29.6 (2013): 2861-2873.

[7] Singh, Bhim, Shiv Kumar Aggarwal, and Tara Chandra Kandpal. "Performance of wind energy conversion system using a doubly fed induction generator for maximum power point tracking." 2010 IEEE Industry Applications Society Annual Meeting. IEEE, 2010.

[8] Muller, Set, M. Deicke, and Rik W. De Doncker. "Doubly fed induction generator systems for wind turbines." IEEE Industry applications magazine 8.3 (2002): 26-33.

[9] Datta, Rajib, and V. T. Ranganathan. "Variable-speed wind power generation using doubly fed wound rotor induction machine-a comparison with alternative schemes." IEEE transactions on Energy conversion 17.3 (2002): 414-421.

[10] Calderaro, V., et al. "A fuzzy controller for maximum energy extraction from variable speed wind power generation systems." Electric Power Systems Research 78.6 (2008): 1109-1118.

[11] Vinothkumar, K., and M. P. Selvan. "Novel scheme for enhancement of fault ride-through capability of doubly fed induction generator based wind farms." Energy Conversion and Management 52.7 (2011): 2651-2658.

[12] Boutoubat, M., L. Mokrani, and M. Machmoum. "Control of a wind energy conversion system equipped by a DFIG for active power generation and power quality improvement." Renewable Energy 50 (2013): 378-386.

[13] Morren, Johan, and Sjoerd WH De Haan. "Short-circuit current of wind turbines with doubly fed induction generator." IEEE Transactions on Energy conversion 22.1 (2007): 174-180.

[14] Tang, Yifan, and Longya Xu. "A flexible active and reactive power control strategy for a variable speed constant frequency generating system." IEEE Transactions on power electronics 10.4 (1995): 472-478.

[15] Fletcher, John, and Jin Yang. "Introduction to doubly-fed induction generator for wind power applications." Paths to sustainable energy (2010): 259-278.

[16] Petersson, Andreas, Lennart Harnefors, and Torbjorn Thiringer. "Evaluation of current control methods for wind turbines using doubly-fed induction machines." IEEE transactions on Power Electronics 20.1 (2005): 227-235.

[17] Seyedi, Mohammed. "Evaluation of the DFIG wind turbine built-in model in PSS/E." (2009).

[18] Abdeddaim, S., and A. Betka. "Optimal tracking and robust power control of the DFIG wind turbine." International Journal of Electrical Power & Energy Systems 49 (2013): 234-242.

[19] Hansen, Kenneth, Christian Breyer, and Henrik Lund. "Status and perspectives on 100% renewable energy systems." Energy 175 (2019): 471-480.